ACOUSTOFLUIDIC SEPARATION OF CARDIOMYOCYTES

Sara Thuresson

2016

LUND UNIVERSITY

Bachelor's Thesis in Biomedical Engineering

Faculty of Engineering LTH

Department of Biomedical Engineering

Supervisor: Maria Antfolk

Examiner: Thomas Laurell

Abstract

Heart failure is one of the most common reasons for death in the modern society. As the field of tissue engineering is evolving, cardiac patches as treatment for suffering patients holds future promise. However, methods for efficient purification of cardiomyocytes from biopsies are lacking, hindering the development of such solutions. Here a novel method for separation of cardiomyocytes in a microfluidic chip is investigated. The separation is based on acoustophoresis, the use of ultrasonic waves in a microfluidic channel to focus particles of different properties, such as size, density and compressibility. Although the method seemed promising, experimental evaluation showed unsatisfactory results. This was mainly due to a lack of well-performing markers to analyze the efficiency of the separation, and concerns that the subpopulations present in the tissue have too similar properties to enable good separation with this method.

Acknowledgements

I would like to extend my thanks to Thomas Laurell for the idea and opportunity to start with this project. Working with this Bachelor's thesis I have learnt much more than microfluidics and acoustophoresis, much owing to the great people at the department, generously sharing their knowledge and experience. Thank you for creating such a welcoming and helpful environment! Special thanks to Maria Antfolk, my supervisor, for teaching me everything from what "balband" is to how science works, to Anke Urbansky for giving me a great crash course on FACS, and to Cecilia Magnusson for guidance in cell issues.

Contents

1. INTRODUCTION

Cardiovascular disease is the leading cause of death in Europe today, with myocardial infarction being one of the most common varieties, accounting for almost half of the total rate of death by cardiovascular disease in Sweden (1). The survivors of myocardial infarction suffer a huge loss of cardiomyocytes in the infarct zone, and as the terminally differentiated cardiomyocytes are not able to regenerate, this results in impaired function of the remaining tissue. Cardiac output in the patient is usually drastically weakened, decreasing life quality. Recent advances in tissue engineering and stem cell research have shown that it is possible to obtain millions of cardiomyocytes derived from embryonic stem cells or induced pluripotent stem cells (2). These derived cardiomyocytes could be cultivated and later transplanted to the patient, *e.g.* as cardiac patches, improving cardiac function and decreasing load on the remaining healthy tissue.

However, high purity of cardiomyocytes is essential for the generation of cardiac patches through tissue engineering, as a well-defined cell population is required. When biopsies are taken, cardiomyocytes therefore need to be isolated from other cells present in the heterogeneous cardiac tissue, such as fibroblasts and endothelial cells. It is critical that viability and cell functionality is preserved during the process, and the recovery rate should be high to maximize efficacy of the isolation. A non-invasive method is preferable, and ideally easy and fast to use.

1.1 THE CARDIAC TISSUE

As mentioned above, cardiac tissue is composed of a heterogeneous cell population with specific functions. Cardiomyocytes compose 20-40% of the cardiac cell population, but occupy 80-90% of the space (3) because they differ from their surrounding cells in size and shape; a human cardiomyocyte is an elongated cell, ranging 15-20 µm in diameter and of varying length (4). The majority of the non-myocytes are fibroblasts, which are smaller and less elongated cells with a size of about 10 µm. Other cells found in the population are endothelial cells and smooth muscle cells, but their fraction of the total population is so small that the isolation of cardiomyocytes often focuses on separating the myocytes from fibroblasts only (5).

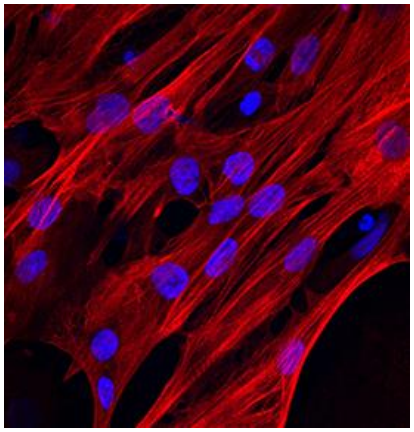

The elongated structure of the cardiomyocytes has evolved to perfect the function of the cells. The cardiomyocytes make up the cardiac muscle, with the primary function to pump blood around the body by beating. The cardiac muscle cells thus must be able to contract and elongate to create these beats, requiring flexibility to stretch the cells enough for a heartbeat (7). The primary function of the fibroblasts in the cardiac tissue is communicating with the cardiomyocytes and secrete components of the extracellular matrix surrounding the cells (8).

Figure 1. Cardiomyocytes derived from human embryonic stem cells. The cell nuclei are stained with DAPI (blue) and the cytoskeleton with NorthernLights™ 557 (red). The elongated structure of the cells is evident. Picture source: (6)

1.2 CURRENT ISOLATION METHODS

Methods used today for isolation of cardiomyocytes from biopsies leave a lot to be desired. A problem is that most markers for cardiomyocytes are intracellular, which makes them inadequate to utilize when the cardiomyocytes are to be used for clinical applications. A newly discovered surface marker for cardiomyocytes, signal-regulatory protein alpha (SIRPA), was used to sort human-induced pluripotent stem cells, but its application for biopsy-retrieved cells remains to be investigated as the efficacy of the marker may differ between these cells (9). A mitochondrial fluorescent dye was reported to be effective for sorting cardiomyocytes (10), but the long-term effects of mitochondrial staining must be further examined before use in clinical applications, and this method may miss out on myocytes with lower mitochondrial content, such as immature human pluripotent stem cells. Instead separation needs to be based on inherent properties of the cardiomyocytes.

An easy and widely used method is called pre-plating, which uses differences in adhesion properties (11). Compared to *e.g.* fibroblasts, the cardiomyocytes take longer time to adhere to a surface of tissue culture. After a certain incubation time, myocytes will therefore stay in suspension whereas non-myocytes such as fibroblasts will have adhered to the surface. This method, however, lacks precision, and neither yield nor purity is high. Usually the procedure is repeated a number of times to increase purity, but these repeated washing steps may damage the cardiomyocytes, resulting in a decreased cell viability.

Another simple method isolates cardiomyocytes based on the difference in density between myocytes and non-myocytes (12). A density gradient is set up in a tube and after centrifugation, the different cell populations will end up in clear bands depending on density. This concept is shown in Figure 2 below. However, the extraction of bands can generally not be perfectly done which lowers purity and recovery rate.

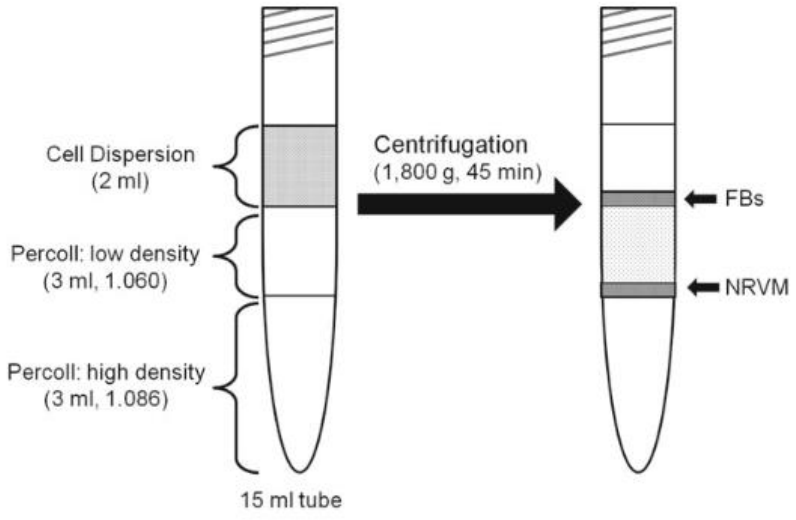

Figure 2. Schematic illustration of Percoll density gradient centrifugation of neonatal rat ventricular myocytes and fibroblasts. A Percoll density gradient is created in a tube, and a cell dispersion with neonatal rat ventricular myocytes (NRVMs) and fibroblasts (FBs) is placed on top. After centrifugation two bands will appear with the two cell populations, due to the density difference of the cells. Reprinted with permission from (12).

An innovative method by Sofla *et al*. used a magnetic field to sort out cardiomyocytes (13). Cardiomyocytes were rendered paramagnetic by adding $NaNO_2$ which oxidizes the myoglobin into metmyoglobin. As the cardiomyocytes are significantly higher in myoglobin content than the other cells in the population, the cells could be sorted in a magnetic field which was actuated in a microfluidic device with different outlets. As magnetic cell sorting is already used in clinical practice today, this may be a good solution. However, the method was only tested for mouse cells, and as the target is to enrich human cardiomyocytes, this method needs further development. Moreover, as the method is not continuous, the yield is low.

As there is a significant size difference between fibroblasts and cardiomyocytes, a few methods based on this fact have been proposed. Murthy *et al*. presented a microfluidic filtering method consisting of a main channel connected to microsieves to isolate the smaller non-myocytes (14). However, this device will face problems with clogging and low throughput because of low flow rates.

Based on the same theory but instead using deterministic lateral displacement (DLD) in a microfluidic system, Zhang *et al*. suggested a method where the steric forces between the cells and the posts in the array resulted in a displacement of the larger cells into the next streamline for each row of posts (15). Connecting the streamlines to separate outlets enabled gathering of the larger cardiomyocytes from one of the outlets. The concept is shown in Figure 3. The device demonstrated fairly low yield (determined as the total number of cells collected from the outlet divided by number of cells in the inlet), 55%, but this could be improved by connecting several devices and running them simultaneously by parallel processing.

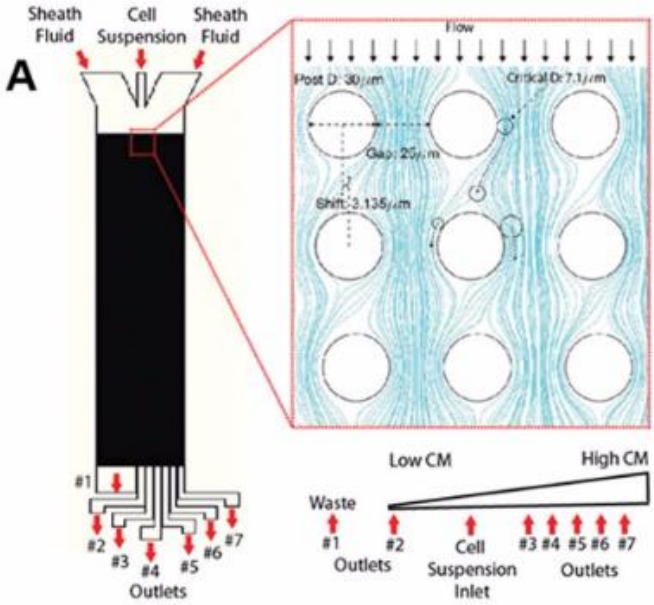

Figure 3. The DLD device designed by Zhang et al. *As the larger cardiomyocytes experience steric forces from the posts in the array, they are displaced into the adjacent streamline. At the end of the device they can be collected from the separate outlets. (15).*

This project has focused on evaluating a method for separating cardiomyocytes based on the size difference between the myocytes and the non-myocytes, *e.g.* fibroblasts. The method, called acoustophoresis, uses ultrasonic standing waves in a microfluidic chip to focus cells of different size into separate positions of the channel, enabling exit in different outlets. Cardiomyocytes can then theoretically be collected from one of the outlets.

1.3 MICROFLUIDICS

The method presented in this project is carried out on a microfluidic scale. Microfluidics is the handling of very small fluid volumes (nano- and microliters) in a chamber of micrometer proportions. Fluids are normally perceived on the macroscale, resulting in a common natural intuition for their behavior. However, on the microscale, common perceptions and knowledge of this will be challenged. At this scale some interesting phenomena, owing to the dominating physics laws, will appear. These will be briefly reviewed below.

1.3.1 INERTIA AND THE REYNOLDS NUMBER

Most fluids on the macroscale experience a turbulent flow. In this case, the flow is chaotic and unpredictable, and adjacent fluid streams will mix rapidly. However, on the microscale, because of the large surface to volume ratio due to the small size of the channels, most flows will instead be laminar. In laminar flow, the viscous forces dominate over inertial forces, making flow stable and predictable. One important consequence is that two adjacent fluid streams will not mix except by diffusion.
The relation between inertial and viscous forces are described by the dimensionless Reynolds number, *Re* in Eq 1(16):

$$Re = \frac{\rho U_0 D_h}{\mu}$$

where ρ is the fluid density, U_0 is the fluid velocity, D_h is the hydraulic diameter of the channel, and μ is the fluid viscosity. For microfluidic channels with water as working fluid, *Re* is typically lower than 10 (17), and laminar flow is generally present in these channels. The transition to turbulent flow usually occurs when *Re* approaches numbers of around 2000-3000.

1.3.2 DIFFUSION AND THE PÉCLET NUMBER

As mentioned above, the consequence of laminar flow is that adjacent fluid streams will only mix by diffusion. On larger scales, the reason for diffusion being insignificant is that the time it takes for a particle to diffuse through a medium is proportional to the square of the distance, $d^2 = 2Dt$, where D is the diffusion coefficient. As the distance d decreases, the time t for diffusion will rapidly decrease. The importance of diffusion will therefore increase on microfluidic length scales, and this can be described by the dimensionless Péclet number, *Pe*, which relates transport by convection to transport by diffusion (17), in Eq 2.

$$Pe = \frac{wU_0}{D}$$

where w is the width of the channel, U_0 is the fluid velocity, and D is the diffusion coefficient.

1.3.3 POISEUILLE FLOW

A pressure-induced fluid flow in a channel will follow a Poiseuille flow (18). This results in a parabolic flow profile, with zero velocity at the channel walls and increasing fluid velocity towards the center. This is depicted in Figure 4.*(19)*

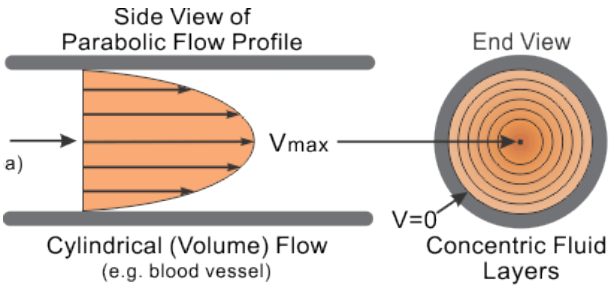

Figure 4. The parabolic flow profile, with higher fluid velocity towards the center, and lower fluid velocity at the channel walls.

1.3.4 STOKE'S DRAG FORCE

Particles moved by an external force in a fluid with low fluid velocity and low Reynolds number, will experience a type of friction, a viscous drag force (18). This is called Stoke's drag force and is described in Eq 3:

$$F_d = 6\pi\mu a v$$

where μ is the dynamic viscosity, a is the particle radius and v is the velocity of the particle.

1.4 ACOUSTOPHORESIS

Acoustophoresis is a microfluidic separation technique which is based on inherent physical properties of the particles. It can be applied to manufactured particles as well as living biomaterial such as cells, since the technique is gentle and conditions such as temperature and surrounding medium in the microfluidic channel can be set to fit the experiment, *e.g.* when working with cells.

1.4.1 THE PHYSICS BEHIND ACOUSTOPHORESIS

The basis for acoustophoretic separation is the primary acoustic radiation force acting on a particle exposed to an acoustic field. The primary radiation force F_{ax} is described by Eq. 4 below (20):

$$F_{ac} = 4\pi a^3 E_{ac} k \sin(2kz)\,\Phi$$

where a is the particle radius, E_{ac} is the acoustic energy density, z is the distance from the pressure anti-node in the axis of the propagating wave, k is the wavenumber ($2\pi f/c_0$) and Φ is the acoustic contrast factor.

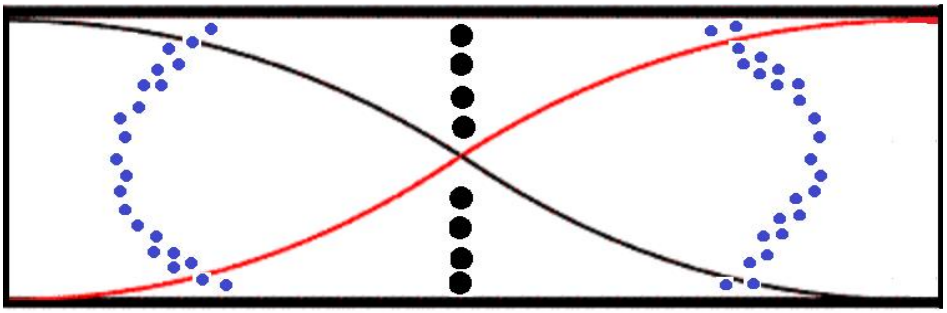

Figure 5. Schematic cross-section of a channel with a width of half the wavelength of the acoustic standing wave. Assuming a positive contrast factor, the smaller blue particles will experience less acoustic force, hence they have not had time to transverse the channel to the same extent as the larger black particles.

To separate particles based on size, note that the size of the force acting on the particles, described in Eq. 4, depends on particle size a^3. If particles of mixed sizes in a suspension will travel through a channel with a standing wave as in Figure 5, the acting force will be larger on the larger particles. Assuming a positive contrast factor, larger particles will experience a larger force towards the pressure node than the smaller particles. Recall that the particles will also be slowed down by the Stoke's drag force (Eq 3), acting against the acoustic force. The velocity of the particle can be derived by balancing these forces so that $F_{ac} = F_{drag}$. The velocity can then be expressed as:

$$v_{rad} = \frac{2\Phi}{3\mu} a^2 E_{ac} k \sin(2kz)$$

The speed at which the particles transverse the channel is proportional to the square of the radius of the particle. At the end of the channel, when a certain amount of time has passed, this results in large particles ending up near the middle and smaller particles closer to the wall. The concept is shown in Figure 5. The slightly bent profile of the band of blue particles arise due to the parabolic flow profile, as the particles closer to the walls have a lower velocity along the channel, thus spending longer time in the channel resulting in a longer exposure time to the radiation force, ending up closer to the center.

However, to achieve separation as in Figure 5, a pre-condition is that the particles are situated close to the walls at the beginning of the channel. This can be solved by introducing a particle-free fluid stream in the center of the channel. Another option is to use pre-focusing, which will be described further in the next section.

Furthermore, as can be seen in Eq. 4, the sign of the acoustic force depends on the acoustic contrast factor Φ which is shown below in Eq. 5 (20):

$$\Phi = \frac{\rho_p + \frac{2}{3}(\rho_p - \rho_0)}{2\rho_p + \rho_0} - \frac{1}{3}\frac{\rho_0 c_0^2}{\rho_p c_p^2}$$

where ρ_p is the density of the particle, ρ_0 the density of the fluid, c_p the speed of sound in the particle and c_0 the speed of sound in the fluid. The acoustic contrast factor thus depends on the

combination of physical properties of the particle and the surrounding fluid. Whether a particle will position itself towards a pressure node or anti-node is determined by the contrast factor. Particles experiencing a negative acoustic contrast factor will move towards the anti-node, whereas a positive factor will make the particles head for the node. Thus particles can also be separated in the channel based on their density and compressibility, shown in Figure 6. If the particles behave similarly in the acoustic field, impeding separation, a solution might be to change the density of the surrounding medium so that the particles display opposite polarity of the acoustic factor, enabling separation as in Figure 6.

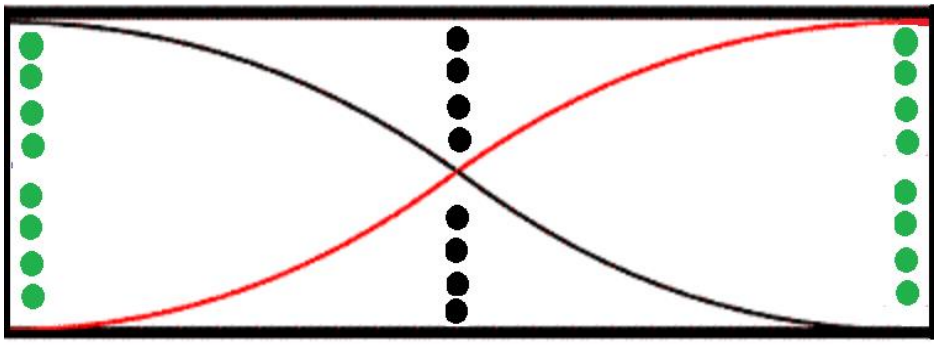

Figure 6. Schematic cross-section of a channel with a width of half the wavelength of the acoustic standing wave. The green particles will experience a negative contrast factor, focusing in the anti-node, whereas the black particles, facing a positive contrast factor, will focus in the middle of the channel.

1.4.2 FREE-FLOW ACOUSTOPHORESIS

Free-flow acoustophoresis uses a continuous laminar flow orthogonal to an acoustic field to separate particles in a microfluidic channel (20). Differently sized particles suspended in a fluid are introduced through an inlet. After positioning the particles along the walls of the channel, particles are separated due to their different migration speed, enabling particles of a certain size, density or compressibility to exit through a specific outlet connected to their trajectories in the channel. Such a concept was early presented by Johnson and Feke in 1995 (21), where it was found that the strength of the applied acoustic field could place the particles in determined paths in the fluid flow inside a chamber. The paths are directed to certain outlets, allowing specific sizes to exit through a specific outlet.

The chamber designed by Johnson and Feke consisted of a transducer and a reflector inside a plexiglass frame, as seen in Figure 7. Today the technique is usually realized in a microfluidic chip of smaller dimensions.

The microfluidic device can be made by silicon, patterned and made by standard photolithography and etching procedures. This is favorable as very precise structures can be fabricated through these procedures. Usually the top of the silicon channel is made by a layer of glass so that visual inspection of the process through a microscope is facilitated.

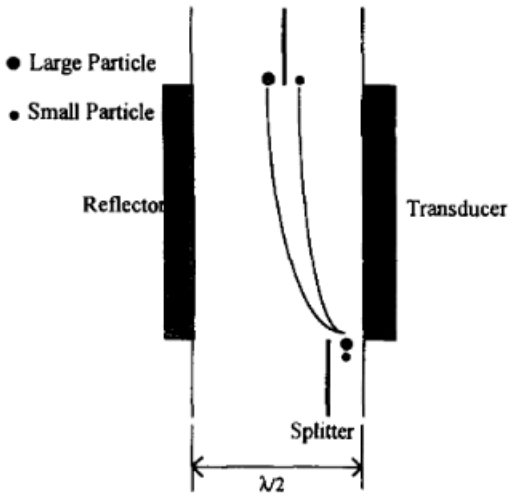

Figure 7. A schematic drawing of the setup by Johnson and Feke. The larger particles traverse the chamber faster than the smaller particles, and can exit through a specific outlet. Reprinted with permission from (21).

Other common materials for microfluidic devices are glass and plastic materials, *e.g.* polydimethylsiloxane (PDMS). However, the softness of PDMS may cause absorption of the sound waves, and also less differences in reflection index between the water and the plastic makes it harder to create a standing wave, which calls for lower flow rates as the acoustic force is weaker.

The channel width is chosen to correspond to a specific wavelength of the acoustic wave, so that there is a definite number of nodes/antinodes. The standing wave is created by a piezo element situated below or above the chip, connected to a function generator. Some of the transferred energy will be lost as heat. This can make the chip heat up considerably if high voltages are applied, which may tamper with the separation performance as *e.g.* the speed of sound (and thus the acoustic wavelength) is temperature-dependent. Temperature control may therefore be a good addition to the setup. This is normally done by connecting a sensor and a Peltier element to the chip, keeping track of the actual temperature and heating/cooling it to the desired temperature level.

The fluid flow in the system can be actuated in several different ways. One approach is to connect a syringe pump system to the chip, controlling flow rates via software determining the pressure of the pumps. Another method is using a pressure system, where the flow rate is created by a fluid pressure in the channel.

To further enhance separation, pre-focusing can be introduced (22). Pre-focusing is two-dimensional, ensuring that particles are aligned not only to a specific position in channel width but also height, changing the scenario in Figure 5 and 6 so that after separation, particles are focused as in Figure 8.

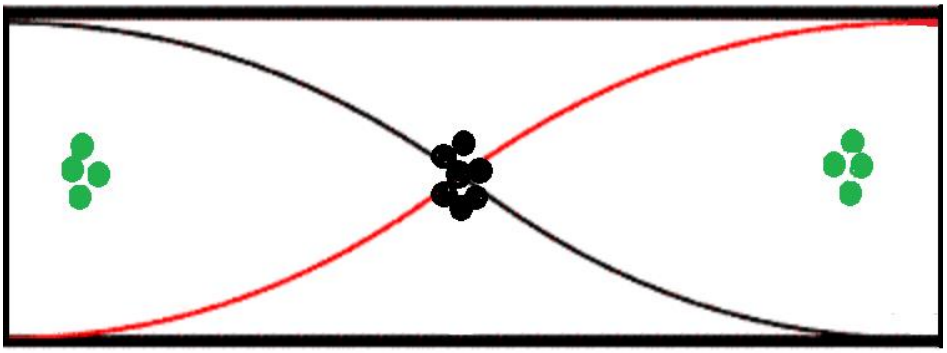

Figure 9. Schematic picture of a cross-section of a channel where separation has been achieved. The particles are now focused in two dimensions, both to the center of the channel height and to a specific position within the acoustic wave.

In this case, two piezo elements are present. The first piezo element is placed below the first part of the channel, where only the mix of particles is present. The wave created by this element is tuned to 2λ/2 over the width of the channel and λ/2 over the channel height, which results in two nodes, and the amplitude is given by the force needed to focus the particles in two dimensions. Assuming positive acoustic contrast factor, particles will focus into the two nodes; this element is thus used to focus the particles into specific positions within the channel before separation, i.e. pre-focusing. This results in all particles being positioned in the same flow velocity regime in the parabolic flow profile, thus having the same speed, which will facilitate separation in the second step. The buffer fluid flow will further improve separation as the buffer forces the particles to the side. The second piezo element can be positioned below the second part of the channel, after the buffer inlet, where separation is initiated. This element is set to create a wave with λ/2 being the width of the channel, as seen in Figure 9 (22), and separation is carried out as described above. The amplitude of this wave is given by the force needed to achieve enough separation.

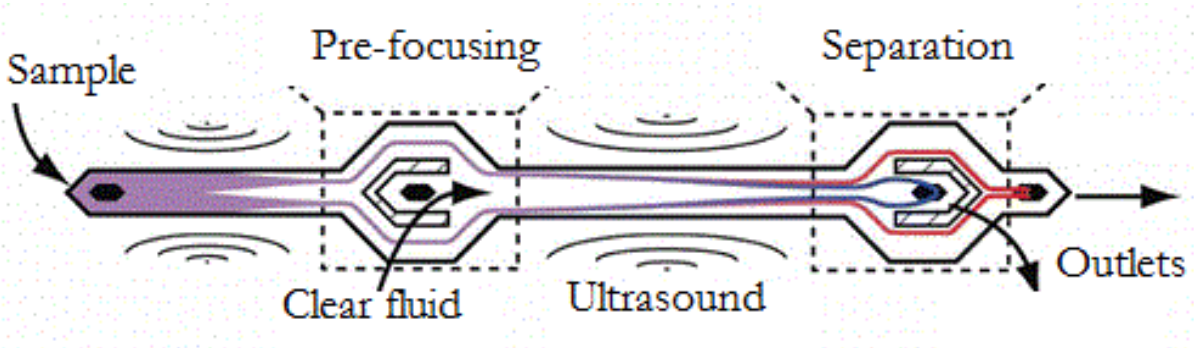

Figure 8. Schematic top view of a double inlet, double-outlet chip for acoustophoresis. The blue and red lines show different trajectories separate particles may take, and the acoustic waves are also displayed. The two sections, prealignment and separation, are indicated. Adapted with permission from (22). Copyright 2012 American Chemical Society.

The advantages for acoustophoresis as a separation method are several. No labelling or sample handling prior to separation is required. It is a gentle, non-contact technique, suitable for rare and delicate cells desired to be kept in a viable state after sorting(23). Due to the microfluidic nature of the technique, small sample volumes are needed, which enables rare cell handling and keeps costs down. By parallel processing and increasing flow rates, throughput can be increased.

There are, however, some limitations to the acoustophoretic method (20). Firstly, there is a lower limit to the particle size that can be affected by acoustic forces. The reason for this limit is that the velocity force is scaled to the particle radius to the power of three (a^3), and at sizes of about 1-2 µm (for a 2 MHz chip) other hydrodynamic forces, such as acoustic streaming, will equal to the primary radiation force, making acoustic separation ineffective. The upper size limit will primarily depend on sedimentation of larger particles.

1.4.3 BIOCOMPABILITY

The biocompability of this method is high, as the surrounding environment in the channel can be controlled to content the cells. Cells have been shown to have sustained viability after the method which opens for clinical applications (23, 24). Biocompability problems that have been discussed are issues concerning temperature and cavitation (23). As mentioned above, the temperature in the channel can rise quickly if higher voltages are applied. However, by controlling the temperature with *e.g.* a Peltier element, this problem can be minimized, and experiments can even be run at 37 degrees, preferred by cells. Cavitation is another matter of concern (23). This tends to form in such flow systems, as *e.g.* air bubbles. When bubbles form and disrupt, local temperature and pressure changes may be drastic. This is usually of no harm to the cells themselves, but might impair the acoustic focusing by changing the local conditions. Ultrasonic waves themselves have been found not to harm cells in this kind of system.

1.4.4 APPLICATIONS

Acoustophoresis has been actualized in several applications. After their first design of a size separating device by Johnson and Feke as described above, the same group demonstrated a proof-of-concept design for separation of hybridoma cells and *Lactobacillus rhamnosus* cells (25) using acoustophoresis with a half-wavelength resonator and laminar flow, although the channel was too large to be defined as a microfluidic channel.

In 2007, Petersson *et al.* presented a design where polystyrene beads of disparate sizes could be separated from each other in an integrated micro-chip, using the technique mentioned above (26). They also reported an efficient way of separating erythrocytes from lipid microemboli, based on the differing acoustic contrast factor of the particles (27). The objective was to remove lipids from blood to avoid embolization of lipid particles in the brain after cardiac surgery, which can cause cognitive dysfunction.

Another interesting application is to separate circulating tumor cells (CTC) from blood. In 2012 Augustsson *et al.* showed separation of prostate cells from white blood cells (22). This is the device depicted in Figure 9. Red blood cells were lysed from whole blood sample, so only white blood cells and prostate tumor cells remained. Prostate tumor cells could then be separated and

enriched because of their difference in size, but also density and compressibility, compared to white blood cells. The method was in 2015 shown to work for other rare CTCs as well, such as breast cancer cells (28). This device was furthermore unique in its ability to concentrate the sample. This application could be useful for helping diagnose the ongoing disease in a cancer patient, to evaluate whether cancer cells are spreading throughout the body. A similar design was used to evaluate the lipid content in raw milk (29), where both lipid enrichment and depletion was possible using two different modes of the standing wave in the system, as shown in Figure 10a and 10b.

Future hopes are that these applications can be connected to trapping and washing devices. By moving cells into clean medium in a separate stream in a channel, a washing method is created.

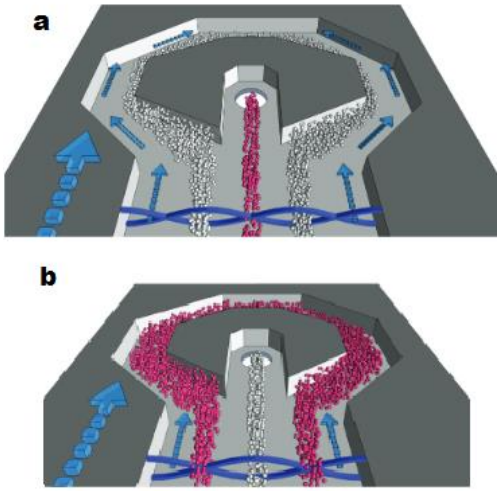

Figure 10 a) Lipid depletion using a 3 λ/2 resonator. The lipid particles (white) focus in the anti-nodes and exit through the side outlet, whereas the residual fraction (red) is collected from the center outlet. b) Lipid enrichment as the lipid particles focus in the center node using a 2 λ/2 resonator. The residual fraction is washed out through the side outlets. Reprinted with permission from (29). Copyright 2009, American Chemical Society.

2.MATERIALS & METHODS

2.1 GENERAL SETUP

The dimensions of the chip are shown in Table 1. A photo of the chip used in this work can be seen in Figure 11.

Table 1. A description of the chip dimensions.

Chip part	Length(mm)	Width (µm)	Depth (µm)
Pre-focusing	20	300	150
Separation	30	375	150

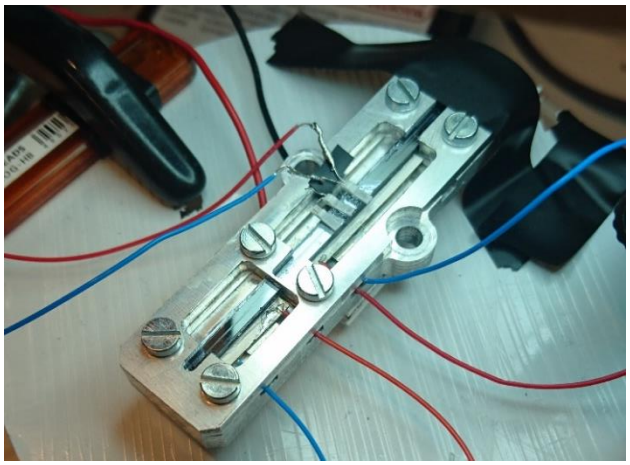

Figure 11. A picture of the chip in the setup used in the experiments. The cables connected are from the function generator to the piezo element (right side of chip), from the sensor to the temperature controller (left side, on top of chip) and from the temperature controller to the Peltier element (left side, beneath chip).

The fluid flow was controlled by syringe pumps (Nemesys syringe pumps, Cetoni GmbH, Germany) and 2 ml plastic syringes (BD, United States). The temperature regulator (TC2812, Cooltronic GmbH, Beinwil am See, Switzerland) connected to the Peltier element (Farnell, London, UK) and Pt1000 resistance temperature sensor (Farnell) (situated on top of the chip), was set to 37 degrees to ensure constant temperature. A function generator (AFG 3022B, Tektronix UK Ltd., Bracknell, UK) and amplifier connected to a piezo element was used to create a wave in the channel. The amplitude and frequency was visualized on an oscilloscope (TDS 2120, Tektronix UK Ltd.).

2.2 CHIP CHARACTERIZATION

The chip used for the experiments was first characterized by performing separation of polystyrene beads of different sizes, to determine optimal frequency settings. Separation of breast cancer cells from white blood cells (WBC) was also attempted as this is known to be feasible (22).

Analysis of the performance was done by flow cytometry (FACS Canto II, BD Bioscience) where populations collected from the different outlets could be visualized by plotting the side scatter (SSC) against the forward scatter (FSC) for the particles, and fluorescence dyes for the cells. The settings used for analysis by flow cytometry was a fixed time (*i.e.* fixed volume) of 60 seconds.

2.2.1 SEPARATION OF POLYSTYRENE BEADS

The beads were blue 3 µm micro-particles based on polystyrene (Sigma Aldrich, Buchs, Switzerland) and 7 µm micro-particles based on polystyrene (Sigma Aldrich). They were suspended in FACS buffer which for 500 ml buffer consists of 490 ml 1x phosphate buffered saline (PBS), 5 ml 20mM ethylene-diamine-tetraacetic acid (EDTA), and 5 ml fetal bovine serum (FBS). FACS buffer was also used as buffer for the second inlet.

2.2.2 SEPARATION OF TUMOR CELLS FROM WBC

For the cancer cell separation experiments, breast cancer cell line MCF7, cultured at the department, was used. Blood was collected from healthy donors, with informed consent, at Skåne University Hospital in Lund, Sweden.

The breast cancer cells were stained with CellTrace™ Oregon Green® 488 (Thermo Fischer) and fixed with 2% PFA. The blood was lysed with BD FACS lysing solution and then the WBC were stained with CD45-APC and fixed with 2% PFA.

The mix of WBC and MCF7-cells, 10x diluted, was suspended in FACS buffer which was also used as buffer from the second inlet.

After separation, the populations were analyzed in the FACS not only with regard to size but also the staining used.

2.3 ISOLATION OF CARDIOMYOCYTES

Human and mouse cardiac tissue was obtained from the cardiology department. The cells were kept in DMEM (Dulbecco's modified eagle medium) on ice prior to acoustophoresis. The cell solution was diluted with FACS buffer before entering of chip, to prevent chip clogging.

An attempt was made to mark the cardiomyocytes with Anti-Cardiac Troponin T-FITC for FACS analysis, which is an intracellular marker. It should be noted that there is lack of well-performing markers for these cells. Other than that, only FSC against SSC was analyzed. The settings used for analysis by flow cytometry was a fixed time (*i.e.* fixed volume) of 60 seconds.

3. RESULTS

Relevant results and pictures are presented below. Calculations can be found in the appendix.

3.1 CHIP CHARACTERIZATION

The chip was characterized in two separate experiments. In the separation of polystyrene beads, a working flow rate was determined, as well as optimal voltage and frequency of the piezo element signal for separation. The tumor cell separation shows performance of the chip with known cells, but unfortunately these results were unsatisfactory.

3.1.1 SEPARATION OF POLYSTYRENE BEADS

The parameters for running the device was determined by visual inspection and results of separation seen in the FACS. These parameters are presented in Table 2. The voltage for separation, at the second piezo, was varied during the experiments to determine optimal amplitude, whereas the following values were held constant after finding the correct parameters.

Table 2. The parameters used when running experiments for finding the optimal separation amplitude.

Flow rate center inlet	80 µl/min
Flow rate side inlet	250 µl/min
Flow rate center outlet	-80 µl/min
Flow rate side outlet	-250 µl/min
Frequency for pre-focusing (1st piezo)	4.960 MHz
Frequency for separation (2nd piezo)	2.037 MHz
Optimal amplitude 1st piezo	5.5 V

After running the device with several different amplitudes on the second piezo element, sample was collected from the center and side outlet and analyzed in the FACS. Below, selected results from one of these analyses is shown. In all pictures, the 7µm particles are in red and the 3µm particles in green. In Figure 12, results from a running with low voltage (4V) is shown.

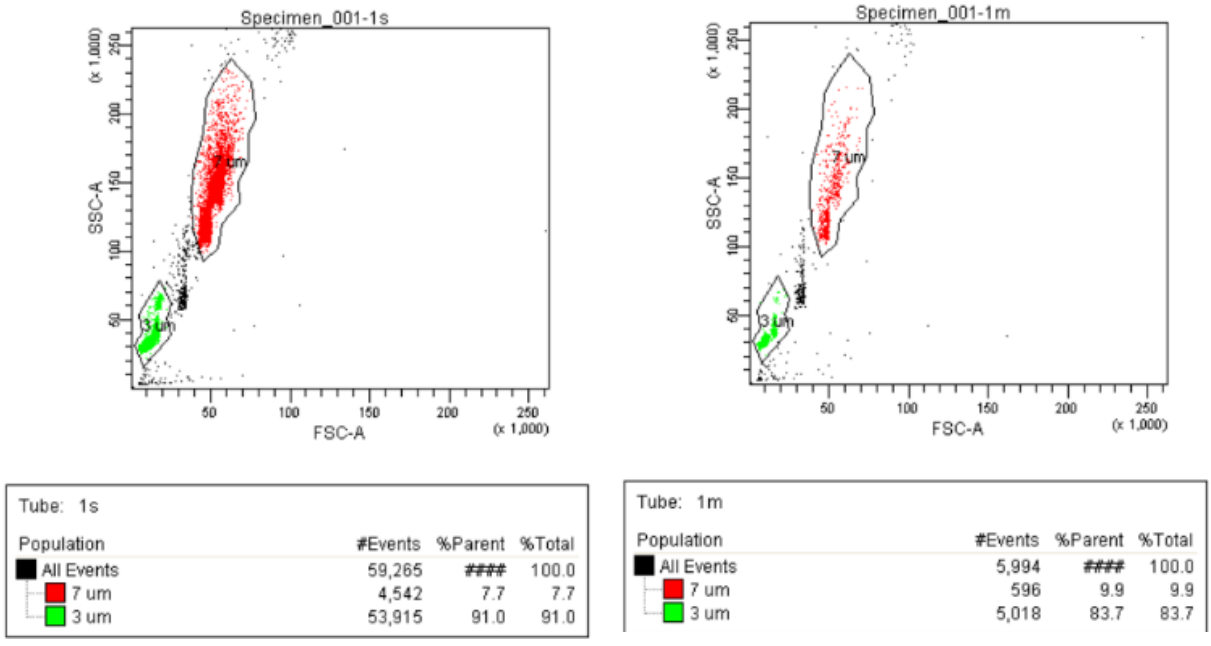

Figure 12. FACS result from running with low voltage (4V), side outlet to the left and center outlet to the right. The total number of events was much higher in the side outlet (about 60'000) than the center outlet (about 6'000).

The number of events is much higher in the sample from the side outlet (left) than the sample from the center outlet (right), indicating many beads exited through the side outlet. It can also be noted that many more 3 µm-beads are present than 7 µm. The particles seen between the populations are most likely doublets, particles that have adhered to each other.

In Figure 13, results from a medium high voltage (6V) are displayed.

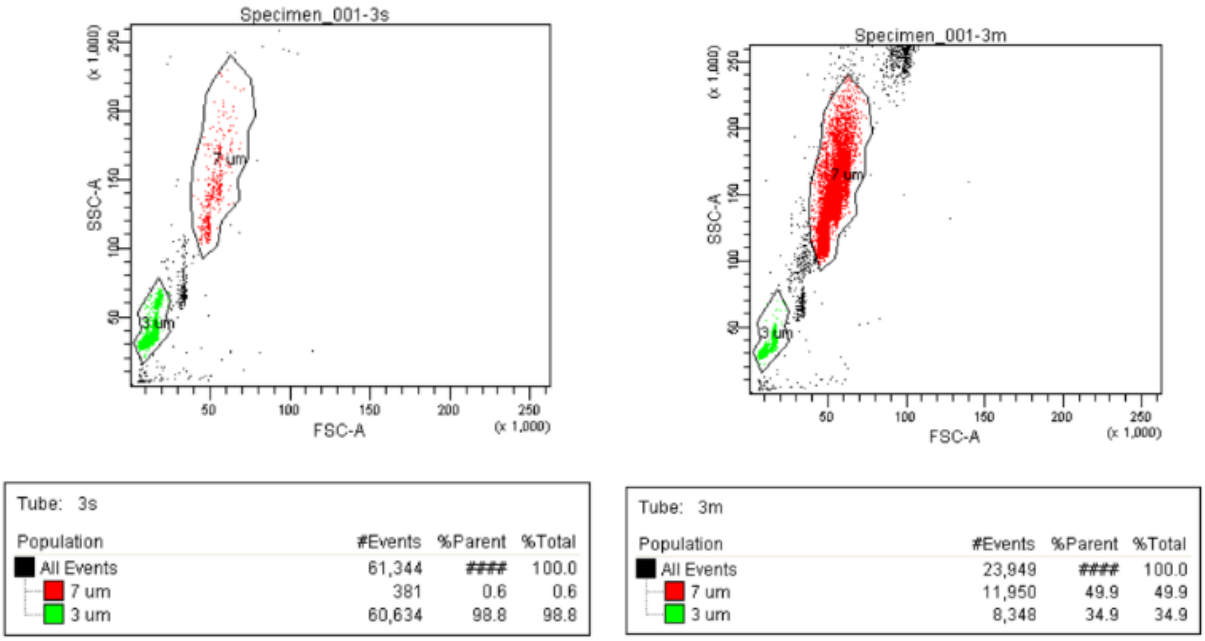

Tube: 3s

Population	#Events	%Parent	%Total
All Events	61,344	####	100.0
7 um	381	0.6	0.6
3 um	60,634	98.8	98.8

Tube: 3m

Population	#Events	%Parent	%Total
All Events	23,949	####	100.0
7 um	11,950	49.9	49.9
3 um	8,348	34.9	34.9

Figure 13. FACS result from running with medium voltage (6V), side outlet to the left and center outlet to the right. In the side outlet sample, more 3 µm-beads were present, about 60'000 to 400 7 µm-beads. In the center outlet, however, about 58% of the beads were 7 µm-beads.

Here it can be seen that in the side outlet (left), many more 3 µm-beads are present than 7 µm (98.8% are 3 µm). In the center outlet (right), the 7 µm-beads are in majority.

In Figure 14, results from a higher voltage (8V) are depicted.

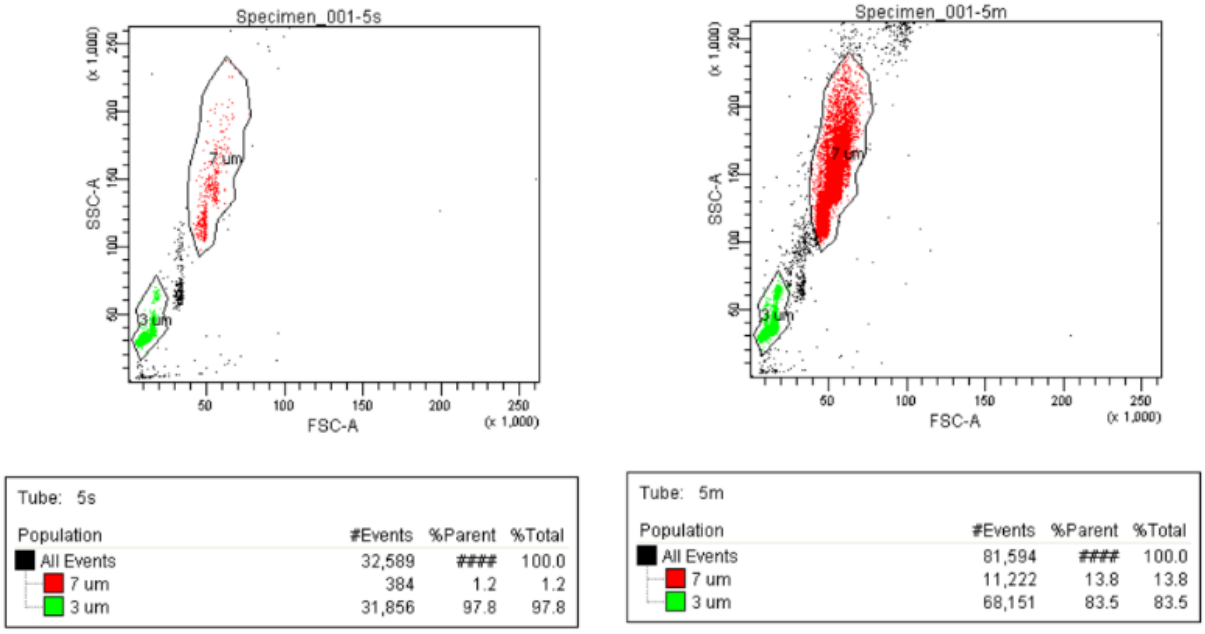

Tube: 5s

Population	#Events	%Parent	%Total
All Events	32,589	####	100.0
7 um	384	1.2	1.2
3 um	31,856	97.8	97.8

Tube: 5m

Population	#Events	%Parent	%Total
All Events	81,594	####	100.0
7 um	11,222	13.8	13.8
3 um	68,151	83.5	83.5

Figure 14. FACS result from running with higher voltage (8V), side outlet to the left and center outlet to the right. The total number of events was higher in the center outlet (about 80'000) than the center outlet (about 30'000).

From Figure 14, it can be noted that the sample from the side outlet (left) gave rise to less events than the center outlet (right), indicating that most beads exited through the center outlet.

After varying the amplitude in several experiments, data from measurements as above was collected to calculate the recovery rate at certain voltage amplitudes, to determine an optimal voltage. Recovery rate was in this case defined as number of events in the center outlet divided by the total number of events in both outlets, and the number of events in the side outlet was multiplied by the dilution factor created by the buffer inlet. The calculations and averaged raw data can be found in appendix. In Figure 15, the results from these calculations are shown as the recovery rates from the center outlet plotted against the voltage amplitude. Bars representing the standard deviation are included. It can be noted that the recovery rate for the 7 µm-beads peaked at a lower voltage, about 6-7V, than for the 3 µm-bead, where the recovery rate started rising at about 9-10V. At about 8V, nearly 100% of the 7 µm-beads exit through the center outlet, but only about 10% of the 3 µm-beads.

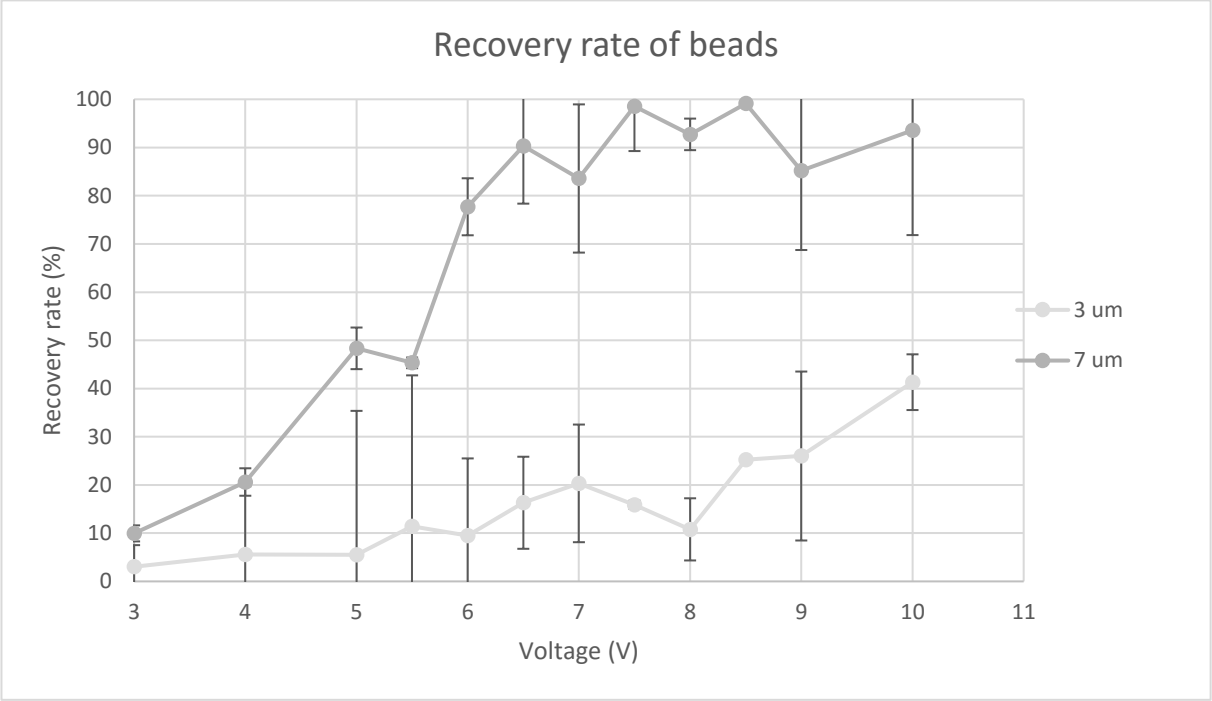

Figure 15. The percentage of beads exiting through the center outlet at different voltages. At about 8V, nearly 100% of the 7 µm-beads exit through the center outlet, but only about 10% of the 3 µm-beads.

3.1.2 SEPARATION OF TUMOR CELLS FROM WBC

During FACS analysis of these experiments, very few tumor cells were detected. A sample taken from the inlet, before separation, only indicated 4-5 tumor cells out of about 60'000 cells in the sample in total, which was lower than the expected number. The FACS picture of this can be found in Appendix. After separation was run, a similar result was obtained.

3.2 ISOLATION OF CARDIOMYOCYTES

During the attempt to separate cardiomyocytes from other cells in the tissue, the same frequency parameters were used as in section 3.1.1. The flow rate was changed to 50 µl/min in the center inlet and 120µl/min in the side inlet (-50 µl/min and -120 µl/min for the outlets, respectively). The voltage for separation was set to 8V. The first result, presented in Figure 16, depicts the populations found in the sample before running it through the device. Two populations can be imagined, but as no markers were available, exact identification is not possible.

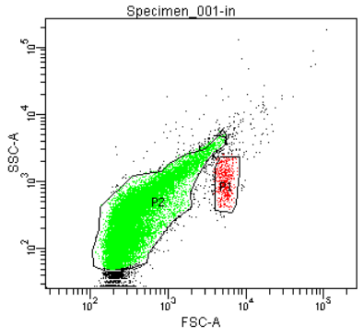

Tube: in			
Population	#Events	%Parent	%Total
All Events	20,000	####	100.0
P1	440	2.2	2.2
P2	18,126	90.6	90.6

Figure 16. FACS picture of the populations in the heart tissue. The red population has a higher FSC (larger size), so this might be the cardiomyocytes.

After running separation in the device, the following results, depicted in Figure 17 and 18, were obtained. Figure 17 shows the populations in the sample collected from the center outlet, and Figure 18 is from the sample collected from the side outlet. Comparing the two pictures, it can be gathered that more particles from the red population exited through the center outlet than the side, and more particles of the green population exited through the side outlet.

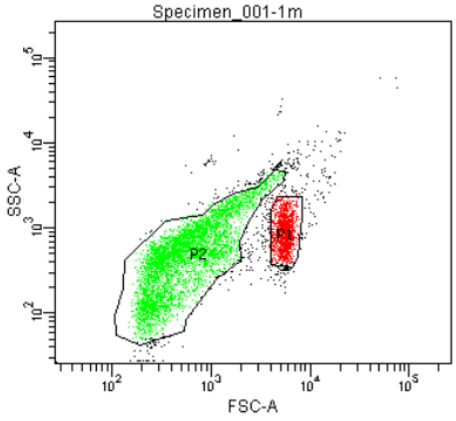

Tube: 1m			
Population	#Events	%Parent	%Total
All Events	5,985	####	100.0
P1	1,216	20.3	20.3
P2	4,284	71.6	71.6

Figure 17. FACS picture of the populations in the sample collected from the center outlet. The red gate shows an event number of 1216, and the green gate has 4284 events, thus rather high percentage red events compared to Figure 17, 22.3% red against 77.8% green events, out of the total population.

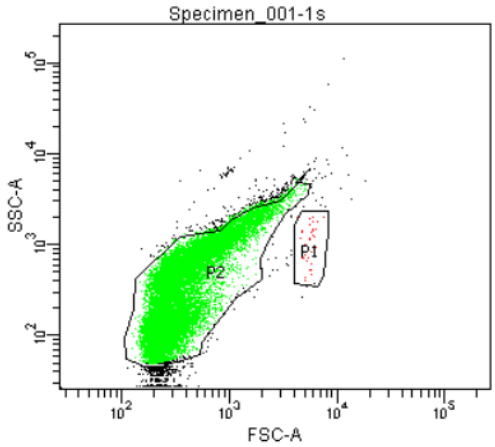

Tube: 1s

Population	#Events	%Parent	%Total
All Events	20,000	####	100.0
P1	39	0.2	0.2
P2	19,103	95.5	95.5

Figure 18. FACS picture of the populations in the sample collected from the side outlet. The red gate shows an event number of 39, and the green gate has over 19000 events, thus nearly no particles from the red population exited through the side outlet.

The recovery rate (number of events in the center outlet divided by the total number of events in both outlets, events in side outlet multiplied by the dilution factor created by the buffer inlet) for both populations is displayed in Table 3.

Table 3. Recovery rates in the two outlets for the red and green population in the previous FACS pictures.

Population	Center outlet (% events)	Side outlet (% events)
Red	92.85	7.15
Green	8.55	91.45

4. DISCUSSION

The main question to answer in this work was whether this method for isolation of cardiomyocytes from heart tissue is satisfactory, and if not, how it could be improved to perform better or if further investigations need to be done. This will be discussed in this section, along with the overall performance of the chip and an evaluation of the experiments conducted.

4.1 CHIP CHARACTERIZATION

The objective for the initial measurements, characterizing the chip, was to find the optimal settings for separating beads that differed in size, and to evaluate the performance of the chip with known particles. These settings were then to be used in the separation of cardiomyocytes in the next part of the work, and the assessed performance to be taken into consideration when discussing the suitability of the method for the desired application.

The optimal frequency of the sound wave created by the piezo elements, the flow rate and the voltage amplitude of the first piezo was, as mentioned above, assessed by visual inspection and by looking at the collected samples in FACS, to estimate separation efficiency. The final parameters were then determined as where separation seemed most effective. More accurate settings could have been obtained by conducting a larger range of these experiments over time and increasing the voltage in smaller steps, *e.g.* in steps of 0.1 V instead of 0.5 V. Furthermore, it would be interesting to find the point where the amplitude is high enough for all beads to exit through the center outlet, a finding that was not made due to concerns that the temperature would rise to inadequate values. The smaller beads may also be too small to be able to focus in this setup. Another experiment that could have been imagined to further examine the performance of the chip is separation of 7 µm-beads and 5 µm-beads. As the size difference is smaller, a good separation of these beads would have indicated a well-performing setup. A major improvement to the conducted experiments would have been to properly measure the initial concentration of beads, before separation, which was unfortunately not done here. This number is also important as the separation performance is affected by the concentration of particles introduced to the system (20).

Separation was achieved at the settings described in the Results section, and the optimal voltage amplitude for the second piezo element would be around 8 V, as this was the point where the difference between the center outlet recovery rate of 7 µm-beads and 3 µm-beads was the largest. In other words, this is where most 7 µm-beads (over 90%) exited through the center outlet and most 3 µm-beads exited through the side outlet (about 90%), indicating a fair separation efficiency.

It can be mentioned that the choice of method for this evaluation, *i.e.* the calculation of recovery rate, was done to evaluate only the separation efficiency at the place of separation and not the recovery of the beads in the chip from inlet to outlet, which this setup was not optimized for.

The chip used had two inlets and two outlets, the second inlet allowing for a buffer flow with the purpose of forcing particles to the side of the channel at the starting point of the separation part. A chip with this layout was chosen to make the separation more stable and enhanced. Simpler versions, with a single inlet, were tested at an early stage in this work but did not perform as well as desired. However, working with a simpler chip has its advantages as there are fewer factors to be concerned about, regarding tubes, choice of buffer etc.

After the attempt to separate breast cancer cells from WBC, a very small number of cells were found in the FACS, for all samples; inlet, center outlet and side outlet. There are at least two possible reasons for this. Either the cells are present, but were not stained properly, which is

why they are invisible in the FACS. The other explanation might be that the cell culture was inappropriately handled, resulting in inviable cells, or perhaps complete removal of the cells during one of the handling steps.

4.2 ISOLATION OF CARDIOMYOCYTES

As there was no functioning way of marking the cardiomyocytes to differentiate them from the other cells in the population, the results from this part are difficult to interpret. An attempt was made to mark the cardiomyocytes with Troponin-T, an intracellular marker (done by *e.g.* Zhang *et. al* (15)), but this was not successful. Due to lack of time the protocol for staining was not optimized and this might be the reason for unsuccessful staining.

However, considering the size difference between fibroblasts and cardiomyocytes, the population in red, which has a larger size according to the forward scatter, might be the cardiomyocytes. If this is the case, a problem can be identified by studying the populations displayed in Figure 16. The size of the cells is reflected by the FSC-axis, and it can be seen that there is an overlap in size between the two populations. In other words, there may be cells in the tissue that are too close to the cardiomyocytes in size to be able to separate them from each other with this method. Moreover, the large number of green particles would pose a problem. On the other hand, the results in Table 3 show recovery rates with a separation close to the values obtained with the beads. Over 90% of the total population in the outlet was red population, with a 10% contamination of the green population, which means that if the red population is the cardiomyocytes, separation might be possible with further experiments. Nevertheless, this population could very well be something else, *e.g.* dead cells or debris, and the cardiomyocyte population may be hidden in the green population, making separation impossible. A fact that strengthens this theory is that the expected ratio between cardiomyocytes and fibroblasts does not comply with the obtained ratio in the inlet-sample acquired in this work.

As heart tissue cells unfortunately only were received a few times during the work, and could only be used the same day or the day after they arrived, there was not enough time for running separation with different dilutions of the cell mix or experimenting with different settings of the separation, such as flow rate or voltage. Clogging of the chip occurred and delayed the process. Due to these factors, not many reliable results could be presented.

4.3 CONCLUSION

A way to separate cardiomyocytes from other cells in the heart tissue could mean creating a path for regenerative medicine to alleviate heart diseases caused by *e.g.* heart failure (30). As heart diseases grow more and more common in the Western society, the implications of such success cannot be underestimated.

The method investigated in this thesis has, in theory, many advantages appropriate for the application and seemed promising. The method is easily integrated with FACS analysis which facilitates analysis, it is gentle to sensitive cells and requires no labelling or sample handling.

However, after experimental trials, doubt remains. The prior problem that needs to be solved is that of the marking; without proper labelling of the cells for analysis, the method cannot be accurately evaluated. From the FACS pictures, two unsatisfying results are available; either the cardiomyocyte population is hidden in the large population marked with green, or it overlaps in size with the other population. Both results could mean that acoustofluidic separation based on size is difficult to accomplish.

Further studies would answer these questions and also investigate other opportunities to separate the cells with a similar method. The mitochondrial fluorescent dye reported by Hattori *et al.* could perhaps solve the problem with labelling (10). One possibility could be to examine whether the compressibility and density differ between the cell populations and if separation thus could be based on this. A sign that this might be a solution is the method described in the Introduction where a Percoll density gradient is used to separate the cells after centrifugation, so the cells must have different density.

An interesting way of combining that method with microfluidics would be to create a density gradient in laminar streams in a microchannel, as suggested by Augustsson *et al* (31). The cells would then align into a stream that corresponds to their density, and if this differs, the cells can be separated into specific outlets just as in conventional acoustophoresis. This could be an alternative and a continuation to this project.

5. APPENDIX

The recovery rate R_r for the center outlet, for a certain population was calculated as

$$R_r = \frac{number\ of\ events\ in\ center\ outlet}{number\ of\ events\ in\ both\ outlets}$$

And for the side outlet it was multiplied with the dilution factor D_f, which for the beads was 250/80 = 3.125 and for the cardiomyocytes 120/50 = 2.4. This is to compensate for the buffer inlet which dilutes the sample a factor that corresponds to the relation between the flow rates. Thus the recovery rate R_r for the side outlet, for a certain population was calculated as

$$R_r = \frac{number\ of\ events\ in\ side\ outlet \cdot D_f}{number\ of\ events\ in\ both\ outlets}$$

The picture obtained from the FACS from the sample with breast cancer cells and WBC can be seen in Figure 19. Population P5 represents the cancer cells which are only 4 out of about 60’000 cells in total (gate P1).

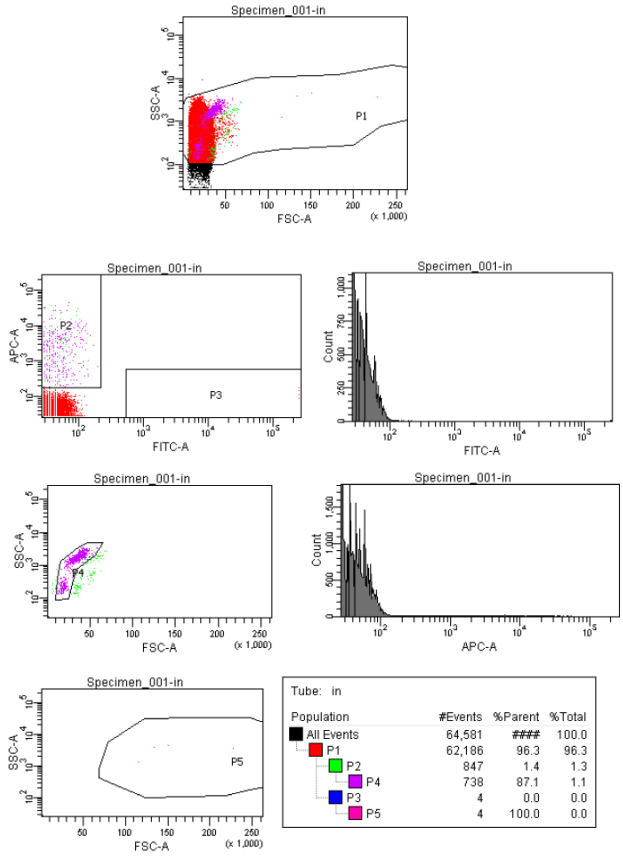

Figure 19. FACS picture of the populations in the sample collected from the sample inlet, before separation. The four cancer cells are found in gate P5, and the total number of cells (including e.g. *WBC) was about 60'000 (gate P1).*

REFERENCES

1. Cardiovascular diseases statistics 2015 [updated 11 December 2015. Available from: http://ec.europa.eu/eurostat/statistics-explained/index.php/Cardiovascular_diseases_statistics#Cardiovascular_healthcare.

2. Laflamme MA, Murry CE. Regenerating the heart. Nature biotechnology. 2005;23(7):845-56.

3. Nag AC. Study of non-muscle cells of the adult mammalian heart: a fine structural analysis and distribution. Cytobios. 1980;28(109):41-61.

4. Adler CP, Friedburg H, Herget GW, Neuburger M, Schwalb H. Variability of cardiomyocyte DNA content, ploidy level and nuclear number in mammalian hearts. Virchows Archiv : an international journal of pathology. 1996;429(2-3):159-64.

5. Naito H, Melnychenko I, Didie M, Schneiderbanger K, Schubert P, Rosenkranz S, et al. Optimizing engineered heart tissue for therapeutic applications as surrogate heart muscle. Circulation. 2006;114(1 Suppl):I72-8.

6. [Available from: https://www.rndsystems.com/products/human-troponin-t-cardiac-antibody-200805_mab1874.

7. Martini FH, Bartholomew, E. Essentials of Anatomy & Physiology. Sixth Edition ed: Pearson; 2011.

8. Sussman MA, McCulloch A, Borg TK. Dance Band on the Titanic: Biomechanical Signaling in Cardiac Hypertrophy. Circulation Research. 2002;91(10):888-98.

9. Dubois NC, Craft AM, Sharma P, Elliott DA, Stanley EG, Elefanty AG, et al. SIRPA is a specific cell-surface marker for isolating cardiomyocytes derived from human pluripotent stem cells. Nature biotechnology. 2011;29(11):1011-8.

10. Hattori F, Chen H, Yamashita H, Tohyama S, Satoh Y-s, Yuasa S, et al. Nongenetic method for purifying stem cell-derived cardiomyocytes. Nat Meth. 2010;7(1):61-6.

11. Iyer RK, Chui J, Radisic M. Spatiotemporal Tracking of Cells in Tissue Engineered Cardiac Organoids. Journal of tissue engineering and regenerative medicine. 2009;3(3):196-207.

12. Golden HB, Gollapudi D, Gerilechaogetu F, Li J, Cristales RJ, Peng X, et al. Isolation of cardiac myocytes and fibroblasts from neonatal rat pups. Methods in molecular biology (Clifton, NJ). 2012;843:205-14.

13. Sofla A, Cirkovic B, Hsieh A, Miklas JW, Filipovic N, Radisic M. Enrichment of live unlabelled cardiomyocytes from heterogeneous cell populations using manipulation of cell settling velocity by magnetic field. Biomicrofluidics. 2013;7(1):014110.

14. Murthy SK, Sethu P, Vunjak-Novakovic G, Toner M, Radisic M. Size-based microfluidic enrichment of neonatal rat cardiac cell populations. Biomedical microdevices. 2006;8(3):231-7.

15. Zhang B, Green JV, Murthy SK, Radisic M. Label-Free Enrichment of Functional Cardiomyocytes Using Microfluidic Deterministic Lateral Flow Displacement. PLoS ONE. 2012;7(5):e37619.

16. David J. Beebe, Glennys A. Mensing a, Walker GM. Physics and Applications of Microfluidics in Biology. Annual Review of Biomedical Engineering. 2002;4(1):261-86.

17. Squires TM, Quake SR. Microfluidics: Fluid physics at the nanoliter scale. Reviews of Modern Physics. 2005;77(3):977-1026.

18. Bruus H. Acoustofluidics 1: Governing equations in microfluidics. Lab on a chip. 2011;11(22):3742-51.

19. [Available from: http://www.cvphysiology.com/Hemodynamics/H006.htm.

20. Lenshof A, Magnusson C, Laurell T. Acoustofluidics 8: applications of acoustophoresis in continuous flow microsystems. Lab on a chip. 2012;12(7):1210-23.

21. Johnson DA, Feke DL. Methodology for fractionating suspended particles using ultrasonic standing wave and divided flow fields. Separations Technology. 1995;5(4):251-8.

22. Augustsson P, Magnusson C, Nordin M, Lilja H, Laurell T. Microfluidic, label-free enrichment of prostate cancer cells in blood based on acoustophoresis. Analytical chemistry. 2012;84(18):7954-62.

23. Wiklund M. Acoustofluidics 12: Biocompatibility and cell viability in microfluidic acoustic resonators. Lab on a chip. 2012;12(11):2018-28.

24. Burguillos MA, Magnusson C, Nordin M, Lenshof A, Augustsson P, Hansson MJ, et al. Microchannel Acoustophoresis does not Impact Survival or Function of Microglia, Leukocytes or Tumor Cells. PLoS ONE. 2013;8(5):e64233.

25. Kumar M, Feke DL, Belovich JM. Fractionation of cell mixtures using acoustic and laminar flow fields. Biotechnology and bioengineering. 2005;89(2):129-37.

26. Petersson F, Aberg L, Sward-Nilsson AM, Laurell T. Free flow acoustophoresis: microfluidic-based mode of particle and cell separation. Analytical chemistry. 2007;79(14):5117-23.

27. Petersson F, Nilsson A, Holm C, Jonsson H, Laurell T. Continuous separation of lipid particles from erythrocytes by means of laminar flow and acoustic standing wave forces. Lab on a chip. 2005;5(1):20-2.

28. Antfolk M, Magnusson C, Augustsson P, Lilja H, Laurell T. Acoustofluidic, label-free separation and simultaneous concentration of rare tumor cells from white blood cells. Analytical chemistry. 2015;87(18):9322-8.

29. Grenvall C, Augustsson P, Folkenberg JR, Laurell T. Harmonic Microchip Acoustophoresis: A Route to Online Raw Milk Sample Precondition in Protein and Lipid Content Quality Control. Analytical chemistry. 2009;81(15):6195-200.

30. Maher KO, Xu C. Marching towards regenerative cardiac therapy with human pluripotent stem cells. Discovery medicine. 2013;15(85):349-56.

31. Augustsson P, Karlsen JT, Su H-W, Bruus H, Voldman J. Iso-acoustic focusing of cells for size-insensitive acousto-mechanical phenotyping. Nature communications. 2016;7.